

# Cation Effect of Bio-Ionic Liquid-Based Electrolytes on the Performance of Zn-Ion Capacitors

Sumana Brahma,<sup>[a]</sup> Jonathan Huddleston,<sup>[a]</sup> and Abhishek Lahiri<sup>\*,[a]</sup>

Zn-ion capacitors (ZICs) are emerging as promising energy storage devices due to their low cost. Currently, aqueous-based electrolytes are primarily used in ZIC which have shown issues related to low Zn deposition/stripping efficiencies, and Zn dendrites formation, resulting in device failure. To overcome these issues and to develop environmentally benign energy storage devices, here we have studied bio-ionic liquid electrolytes (bio-ILs) in both symmetric and asymmetric capacitors. Choline acetate (ChOAc) and betaine acetate (BetOAc) in water were investigated as electrolytes for capacitors in the presence and absence of Zn salts. Spectroscopic analysis showed that Zn solvation in the electrolytes changes significantly with the change in cation which affects the electrochemical reactions

and capacitor performance. Raman analysis showed the Zn complex formed in the case of ChOAc is  $[\text{Zn}(\text{OAc})_4]^{2-}$  whereas for BetOAc is  $[\text{Zn}(\text{OAc})_5]^{3-}$  thereby the Zn deposition/stripping in ChOAc-based electrolyte is quite stable whereas in case of BetOAc, Zn deposition/stripping is unstable. In the ChOAc electrolyte, the Zn/activated carbon asymmetric cell showed a capacity of  $>90 \text{ Fg}^{-1}$  at  $0.1 \text{ Ag}^{-1}$  and a capacitance close to  $40 \text{ Fg}^{-1}$  at  $0.5 \text{ Ag}^{-1}$  with  $\sim 82\%$  capacity retention after 3000 cycles, whereas BetOAc could only be used in symmetric cell capacitor. This study shows that bio-ILs can be used as sustainable electrolytes in energy storage devices wherein the cation plays a significant role in the capacitor performance.

## Introduction

Due to intermittent electricity production from renewable sources, energy storage devices such as hybrid supercapacitors (SCs) or dual-ion batteries are being investigated.<sup>[1,2]</sup> Li-ion-based hybrid SCs and dual-ion batteries have been extensively studied in industries and academic research fields.<sup>[3,4]</sup> However, due to the limitation of Li resources, and difficulty in recycling, alternative elements for energy storage devices, such as  $\text{Na}^+$ ,  $\text{K}^+$ ,  $\text{Mg}^{2+}$ ,  $\text{Zn}^{2+}$ ,  $\text{Al}^{3+}$ , etc. are being investigated.<sup>[5–11]</sup> Among all the mentioned metal-ion hybrid capacitors, Zn-ion capacitors (ZIC) are regarded to be the most encouraging candidate owing to their high theoretical capacity ( $819 \text{ mAhg}^{-1}$ ), multi-electron reaction material, high energy density, low oxidation-reduction potential ( $-0.76 \text{ V}$  vs SHE), economic viability and good compatibility of Zn with water etc.<sup>[12,13]</sup> ZICs comprise a capacitor-type cathode (physical adsorption), battery-type anode and an electrolyte containing Zn ions. Carbon-based cathodes have been studied in ZICs as they have high charge storage capability, outstanding electrical conductivity, tuneable pore structure, high surface area and are abundant.<sup>[14–18]</sup>

However, the ZICs or zinc ion batteries (ZIB) with aqueous electrolytes frequently encounter several complications, includ-

ing fast capacity deterioration, low Coulombic efficiency, low Zn anode deposition/stripping efficiency and Zn dendrites formation.<sup>[19,20]</sup> Moreover, acidic Zn-ion capacitors with acidic electrolytes are also confronted with several safety issues.<sup>[19]</sup> Therefore, electrolytes play an essential role for ZIC and ZIB devices and it is vital to tune a novel electrolyte with a wide electrochemical window having good compatibility with Zn anode and carbon-based cathode, high ionic conductivity, and which inhibits Zn dendrite formation.<sup>[21,22]</sup> Furthermore, to enhance the performance of the ZIB or ZIC, the morphology of Zn deposition should be smooth and homogenous.

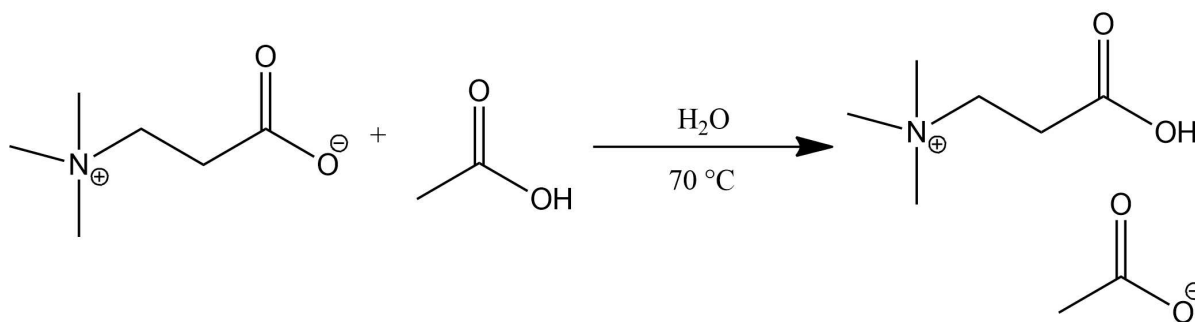
Compared to aqueous electrolytes, little has been studied with ionic liquid (IL) electrolytes in ZICs and ZIBs. ILs possess low vapour pressure, high thermal stability, high electrical conductivity, and a wide electrochemical window.<sup>[23,24]</sup> Moreover, in ILs the solvation of metal ions can be tuned based on the cations and anions on the ILs which would then affect the electrochemical behaviour and electrodeposition process.<sup>[25–27]</sup> Furthermore, water addition can efficiently enhance the polarity, viscosity, ionic conductivity, surface tension, interfacial properties and electrochemistry.<sup>[28–30]</sup> Therefore, it is possible to enhance the performance of ZICs in IL/water electrolytes. For instance, Chen et al. showed that 1-butyl-3-methylimidazolium trifluoromethanesulfonate ([BMIM]OTF) IL/water has antifreezing ability for ZIC even at  $-30^\circ\text{C}$ .<sup>[31]</sup> Liu *et al.* showed a Zn/graphite hybrid capacitor with choline acetate (ChOAc)/water electrolyte that delivers a high energy density of  $53 \text{ Wh kg}^{-1}$  at a power density of  $145 \text{ W kg}^{-1}$ .<sup>[32]</sup>

However, the environmental toxicity and low biodegradability of ILs have restricted their applicability in wearable and implantable devices.<sup>[33]</sup> Therefore, research on synthesizing novel bio-IL structures which are derived from biomolecules such as amino acids vitamins, carbohydrates etc.<sup>[34,35]</sup> are being

[a] S. Brahma, J. Huddleston, A. Lahiri  
 Department of Chemical Engineering, Brunel University London, Uxbridge  
 UB8 3PH  
 E-mail: abhishek.lahiri@brunel.ac.uk

Supporting information for this article is available on the WWW under  
<https://doi.org/10.1002/celec.202400511>

© 2024 The Authors. ChemElectroChem published by Wiley-VCH GmbH. This is an open access article under the terms of the Creative Commons Attribution License, which permits use, distribution and reproduction in any medium, provided the original work is properly cited.



Scheme 1. Synthesis of BetOAc.

investigated. Compared to aprotic ILs, bio-ILs are biodegradable and biocompatible making them attractive sustainable electrolytes for energy storage applications.<sup>[36,37]</sup> Furthermore, these bio-ILs can be easily synthesized and economically cheaper than their aprotic counterparts. Some recent studies have shown the feasibility of bio-ILs in Zn batteries. Kao-ian *et al.* has demonstrated that Zn ion battery with bio-IL based deep eutectic solvent electrolyte showed a high capacity of 170 mAh g<sup>-1</sup> at 50 mA g<sup>-1</sup>.<sup>[38]</sup> Lahiri *et al.* exhibited another Zn ion battery with polypyrrole/Zn composite and choline-based bio-IL which showed 130 mAh/g at 200 mA g<sup>-1</sup>.<sup>[39]</sup>

In the present paper, we have investigated the cation effect of bio-ILs; choline acetate (ChOAc) and betaine acetate (BetOAc) in water and its effect on symmetric and asymmetric capacitors in the presence and absence of Zn salts. Spectroscopic studies were performed to understand the Zn solvation chemistry which was then correlated with Zn deposition and stripping processes and the capacitor performance. It was observed that cation is responsible for change in Zn solvation structure which changes the Zn electrochemistry and Zn-ion capacitor performance.

## Experimental Section

### Materials

Choline acetate (ChOAc) 98%, betaine 99.5%, acetic acid, zinc acetate (Zn(OAc)<sub>2</sub>) 98%, N-methyl pyrrolidine (NMP), polyvinylidene fluoride (PVDF), and super-p were used as received from Sigma-Aldrich. Activated carbon (90 nm particle size) was procured from Nanografi Nano Technology, Germany.

### Synthesis of BetOAc

Betaine (10 mmol) was added to 250 mL water in a round bottom flask. Then the acetic acid was added dropwise. The reaction mixtures were stirred at 70 °C for 24 h under N<sub>2</sub> atmosphere. The preparation of BetOAc is shown in Scheme 1. The solvent water in the reaction mixture was removed by rotavapour. The obtained solid was further washed with chloroform. The final crude products were dried at 80 °C under vacuum for 48 h and stored in N<sub>2</sub> atmosphere. The prepared BetOAc were characterized by <sup>1</sup>H and <sup>13</sup>C NMR spectroscopy (Supporting information Figure S1 and S2).

### Apparatus and Procedure

The <sup>1</sup>H NMR and <sup>13</sup>C NMR were recorded in Bruker Avance 500 MHz spectrometer with D<sub>2</sub>O as an external solvent. The Raman spectra of 80% ChOAc/water, 80% BetOAc/water and 1 mol L<sup>-1</sup> Zn(OAc)<sub>2</sub> in 80% ChOAc/water and 80% BetOAc/water were analysed in Renishaw via confocal Raman microscope, equipped with a 514 nm laser (Stellar-REN) and using a diffraction grating of 1800 lines/mm with a Renishaw CCD camera as the detector, respectively. For Raman, the samples were run with laser power at 100% using the 5x objective lens with a 532 nm laser, respectively.

The viscosity of ChOAc and BetOAc electrolytes were measured in Anton Parr AMVn viscometer and was found to be 82 mPas and 3.67 mPas, respectively at 22 °C. The ionic conductivity of the electrolyte was estimated using Mettler Toledo ionic conductivity measurement system and was found to be 2.54 mS cm<sup>-1</sup> and 25.5 mS cm<sup>-1</sup> for ChOAc and BetOAc electrolytes, respectively.

For developing the carbon electrodes, a homogeneous slurry was obtained by mixing AC (90%), PVDF (5 wt.%) and super-P carbon (5 wt.%) in NMP solvent. The slurry was coated onto a graphite foil by doctor blading with a mass loading of 2 mg cm<sup>-2</sup>. All the electrochemical measurements, including the cyclic voltammetry (CV), and galvanostatic charge-discharge (GCD) were conducted employing the Biologic model VSP-3E potentiostat controlled by EC lab software. For symmetric cells (AC|Bio-IL electrolytes-soaked glass fibre|AC), the CV and the GCD were carried out in 80% ChOAc/water, 80% BetOAc/water, 80% ChOAc/water containing 1 M Zn(OAc)<sub>2</sub>, and 80% BetOAc/water containing 1 M Zn(OAc)<sub>2</sub> electrolytes. For asymmetric devices, AC|bio-IL electrolytes-soaked glass fibre|Zn was used with 80% ChOAc/water/1 M Zn(OAc)<sub>2</sub> electrolytes.

From the obtained data, the specific capacitance of the cell ( $C_{\text{spec, cell}}$ ) was calculated based on the Equation (1).<sup>[40]</sup>

$$C_{\text{spec, cell}} = \frac{I \Delta t}{m_{\text{tot}} \Delta V} \quad (1)$$

Where  $m_{\text{tot}}$  (g) is the total mass of the active material (AC),  $I$  (A) is the applied current,  $\Delta V$  (V) is the potential range, and  $\Delta t$  (s) is the discharging time.

The energy density ( $E_{\text{cell}}$ ) (Wh kg<sup>-1</sup>) and power density ( $P_{\text{cell}}$ ) (W kg<sup>-1</sup>) of the cell were determined using Equation (2) and (3).<sup>[41]</sup>

$$E_{\text{cell}} = \frac{C_{\text{spec, cell}}}{7.2} \Delta V^2 \quad (2)$$

$$P_{cell} = \frac{E_{cell}}{\Delta t} \quad (3)$$

## Results and Discussions

### AC/AC Symmetric SCs

To understand the electrochemical behaviour of AC electrodes in 80% ChOAc/water and 80% BetOAc/water, symmetric cells were studied. The CV profiles of AC in 80% ChOAc/water and 80% BetOAc/water are shown in Figure 1a and Figure 1b respectively. The potential was scanned from 0–1.5 V at different scan rates in the range of 1–100 mVs<sup>-1</sup>. The CV becomes irreversible if the potential is scanned beyond 1.5 V, possibly due to the decomposition of water. The symmetric rectangular-shaped CV curves of AC in both ChOAc and BetOAc electrolytes at different scan rates (1–100 mVs<sup>-1</sup>) reveal the ideal capacitive nature of the symmetric cell. Comparing the CV curves, it is evident that for BetOAc electrolyte, the area under the curve is higher than ChOAc. In general, the conductivity and viscosity of the ILs decrease with an increase in chain length, which would undermine the capacitance and rate performance.<sup>[42]</sup> However, here the opposite trend is observed which may be due to the effect of cation chain length orientation and the compatibility of the betaine chain length size with AC.<sup>[43]</sup>

Furthermore, all the GCD curves (Figure 1c and 1d) at various current densities in the voltage window of 0–1.5 V exhibit symmetric triangular shapes. The  $C_{spec,cell}$  at different current densities are measured using Equation (1) and plotted in Figure 1e, which shows a decrease in the specific capacitance from 55 Fg<sup>-1</sup>–9 Fg<sup>-1</sup> when the current density varies from 0.1 Ag<sup>-1</sup>–3 Ag<sup>-1</sup> for BetOAc, whereas in the case of ChOAc the

specific capacity decreases from 25 Fg<sup>-1</sup>–7 Fg<sup>-1</sup>. The error estimation of the specific capacitance for both ChOAc and BetOAc systems were  $\pm 5$  Fg<sup>-1</sup>. The AC/AC symmetric SC devices have a somewhat lower capacity than the other reported SC devices in aqueous electrolytes, but this result is comparable with the SC devices with ILs as electrolytes.<sup>[32,44,45]</sup> Moreover, the device with 80% BetOAc/water demonstrates the stability of 82% capacitance retention even after 2000 GCD at 0.5 Ag<sup>-1</sup> whereas 99% capacitance retention is observed in the case of 80% ChOAc/water system. (Figure 1f).

### Symmetric AC/AC SCs with Bio-ILs in the Presence of Zn Salt

To understand the effect of Zn salt in the SC devices, a symmetric SC device was fabricated with 80% ChOAc/water/1 M Zn(OAc)<sub>2</sub> and 80% BetOAc/water/1 M Zn(OAc)<sub>2</sub> electrolytes. The CV carried out in the scan rate range of 1–100 mVs<sup>-1</sup> (Figure 2a and 2b) for both the electrolytes show that the capacitive nature of AC is retained in the presence of Zn salt even at 100 mVs<sup>-1</sup>. However, it was observed that the specific capacitance drastically reduced after adding Zn(OAc)<sub>2</sub>. ChOAc-based electrolyte showed a maximum specific capacitance of 38 Fg<sup>-1</sup> at 1 mVs<sup>-1</sup> scan rate whereas the BetOAc system exhibits 27 Fg<sup>-1</sup> at the same scan rate. All the GCD curves (Figure 2c and 2d) at various current densities (0.1 Ag<sup>-1</sup>–3 Ag<sup>-1</sup>) within the same voltage window of 0–1.5 V exhibit symmetric triangular shapes. The measured  $C_{spec,cell}$  at different current densities for both the electrolytes are plotted in Figure 2e, which indicate a decrease in the specific capacitance from 20 Fg<sup>-1</sup>–3 Fg<sup>-1</sup> for ChOAc system whereas 14 Fg<sup>-1</sup>–2 Fg<sup>-1</sup> for BetOAc system when the current density varies from 0.1 Ag<sup>-1</sup>–3 Ag<sup>-1</sup>. Interestingly, in the presence of Zn(OAc)<sub>2</sub>, the opposite

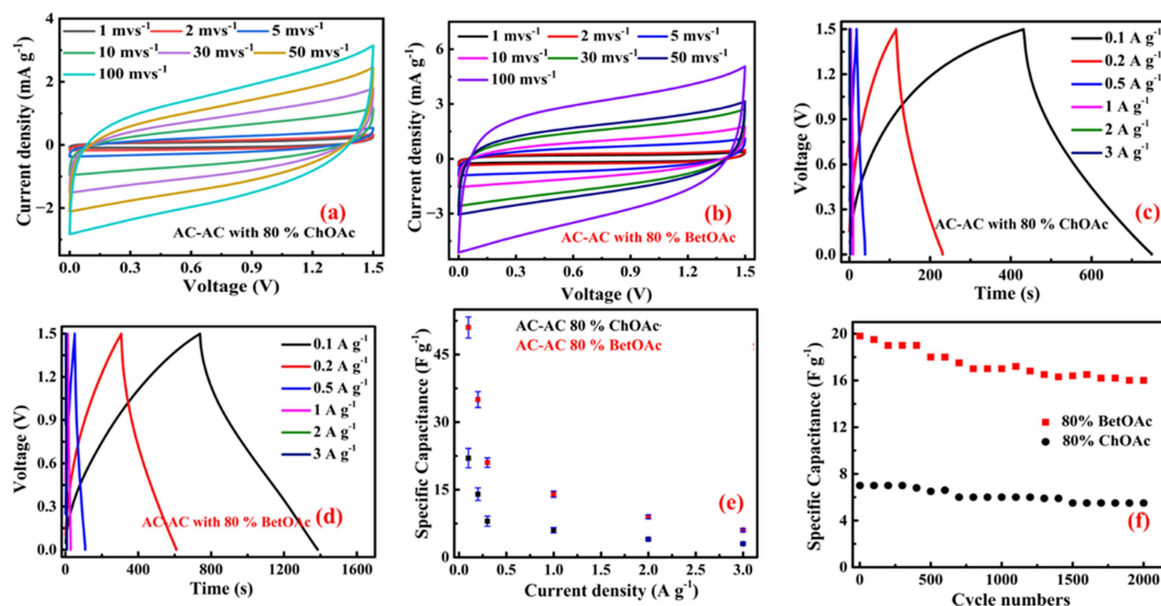


**Figure 1.** (a), (b) CV Curve at different scan rates in (c), (d) GCD profile at different current densities, (e) The specific capacity of the capacitor at different current densities along with error estimated as a function of different current densities (f) Cyclability of AC/AC symmetric device in 80% ChOAc/water and 80% BetOAc/water electrolyte systems.

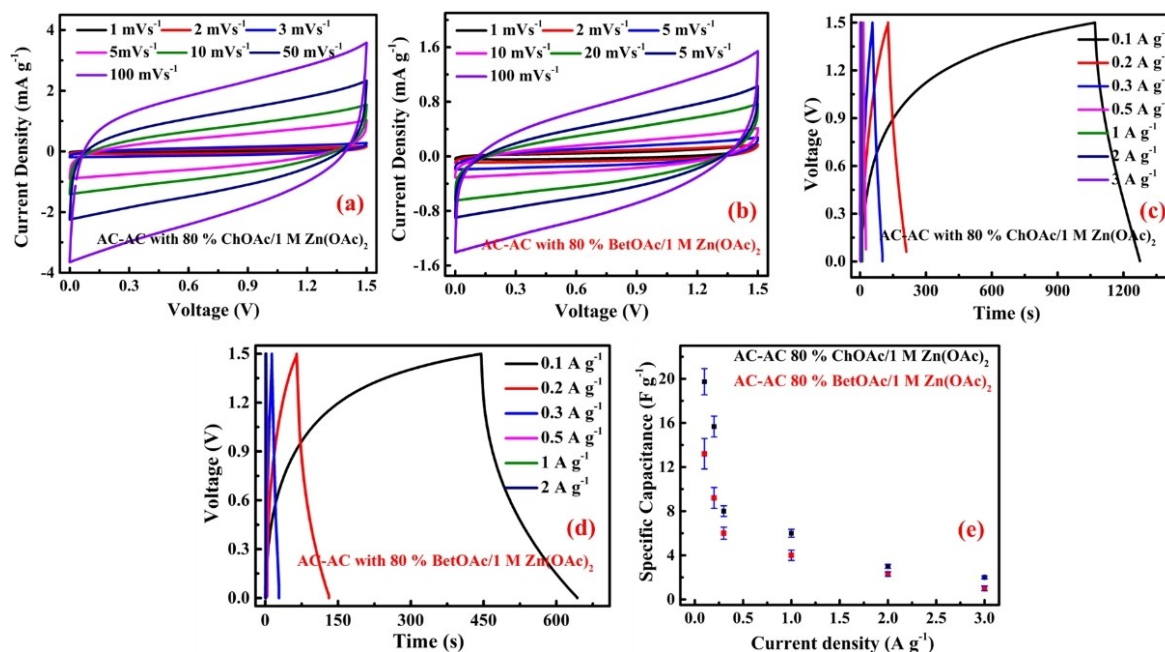


**Figure 2.** (a), (b) CV Curve at different scan rates in (c, d) GCD profile at different current densities, (e) The specific capacity as a function of different current densities of AC/AC symmetric device in 80% ChOAc/water/1 M Zn(OAc)<sub>2</sub> and 80% BetOAc/water/1 M Zn(OAc)<sub>2</sub> electrolyte systems.

trend in capacity is observed where ChOAc system shows higher specific than BetOAc, which might be due to the change in Zn coordination in the complex formed with ChOAc and BetOAc.<sup>[46]</sup>

To understand the Zn solvation, IR and Raman of the electrolytes were performed. Figure 3 compares the IR spectra of ChOAc and BetOAc with and without 1 M Zn(OAc)<sub>2</sub>. For the case of ChOAc, prominent peaks between 1200 and 1800 cm<sup>-1</sup> are observed. For ChOAc, the 1385 cm<sup>-1</sup> can be related to the CH<sub>3</sub> vibration of Choline and the peak at 1568 cm<sup>-1</sup> can be attributed to carbonyl vibration in the acetate anion.<sup>[46,47]</sup> On

addition of water to choline acetate, these peaks shift to 1403 and 1556 cm<sup>-1</sup> and an additional peak at 1645 cm<sup>-1</sup> is observed which can also be associated with free acetate.<sup>[46]</sup> The addition of 1 M Zn(OAc)<sub>2</sub> does not show much change in the vibration modes of methyl or acetate, but the 1645 cm<sup>-1</sup> peak changes to a shoulder which can be related to the Zn coordinating with the acetate.<sup>[48]</sup> In comparison, the prominent peak at 1331 cm<sup>-1</sup> for betaine acetate-water electrolytes can be attributed to the vibration of the bond between -CH<sub>2</sub>N<sup>+</sup>(CH<sub>3</sub>)<sub>3</sub> group of Betaine and the OH<sup>-</sup>.<sup>[49]</sup> Due to the change in the cation-anion interaction, the carbonyl vibration in acetate is observed at

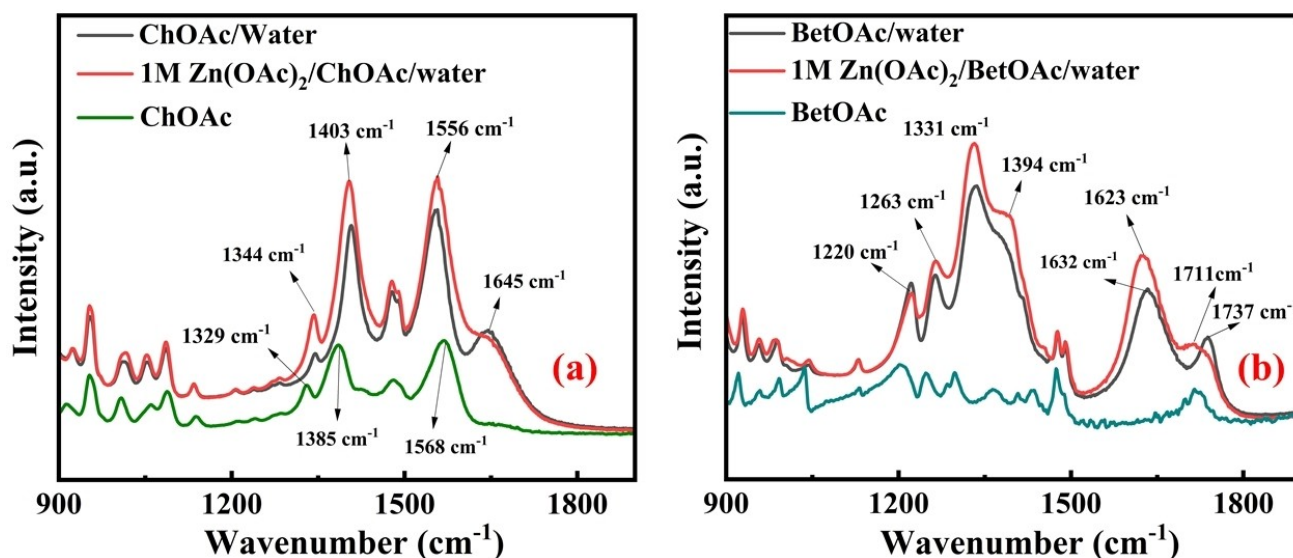


**Figure 3.** FTIR spectra of (a) ChOAc, ChOAc/water and ChOAc/water/1 M Zn(OAc)<sub>2</sub> (b) BetOAc, BetOAc/water and BetOAc/water/1 M Zn(OAc)<sub>2</sub>.

1632  $\text{cm}^{-1}$  and 1737  $\text{cm}^{-1}$  compared to 1556  $\text{cm}^{-1}$  and 1645  $\text{cm}^{-1}$  which occurs for Choline acetate. In addition to  $\text{Zn}(\text{OAc})_2$ , a peak shift to 1623  $\text{cm}^{-1}$  and 1711  $\text{cm}^{-1}$  of the carbonyl group is observed and can be attributed to Zn coordinating with acetate. Based on the IR spectra, it is evident that for betaine cation, Zn coordination results in a stronger vibrational shift.

To understand the Zn coordination with acetate, Raman spectroscopy was performed. Figure 4 compares the Raman spectra between 900 and 1000  $\text{cm}^{-1}$  from which the 'free' acetate and coordinated acetate can be evaluated.<sup>[48,50]</sup> In the case of ChOAc, on the addition of 1 M  $\text{Zn}(\text{OAc})_2$  peak broadening and a shoulder is observed at 920  $\text{cm}^{-1}$  which can be associated with coordination of  $\text{Zn}(\text{OAc})_2$  with ChOAc. Besides, slight change in the Choline peak at 955  $\text{cm}^{-1}$  is observed. In comparison, for BetOAc, a shift in the peak at 930  $\text{cm}^{-1}$  is observed and a decrease in intensity is observed at 960  $\text{cm}^{-1}$  which is related to betaine cation. On curve fitting the Raman with Voigt function, the coordination number was evaluated using Equation (4).

$$N = \frac{A_{\text{CO}}/A_t}{x} \quad (4)$$

Where  $A_{\text{CO}}$  and  $A_t$  are the peak areas of coordinated and free anion, respectively and  $x$  is the mole fraction of  $\text{Zn}^{2+}$  ion to total acetate ions. For ChOAc, the calculated average number of acetate coordinated to each  $\text{Zn}^{2+}$  was found to be 4.3 whereas for BetOAc, it was found to be 4.8 which suggests that the Zn complex formed in the case of ChOAc is  $[\text{Zn}(\text{OAc})_4]^{2-}$  whereas for BetOAc is  $[\text{Zn}(\text{OAc})_5]^{3-}$ . The possible chemical reactions of  $\text{Zn}(\text{OAc})_2$  with Choline and Betaine acetate is shown in Figure 4e and f. Previous investigations have shown that anions affect the Zn deposition potential which is related to the

difference in coordination of Zn ions.<sup>[51,52]</sup> However, interestingly, here we find that cations can also change the Zn solvation structure.

To understand the effect of Zn solvation on Zn electrochemistry, experiments were carried out to understand the Zn deposition on Cu and Zn electrodes from the two electrolytes. The CV of Zn on Cu from the two electrolytes are shown in Figure 5. From Figure 5a, the cathodic scan shows a reduction process below 0.05 V from Zn containing ChOAc electrolyte which is related to deposition of Zn on Cu. In the anodic scan, an oxidation peak at 0.2 V is observed due to the Zn oxidation/dissolution process. In comparison, for Zn deposition from BetOAc (Figure 5b) a wide reduction peak commencing at 0.7 V is observed in the cathodic scan which peaks at -0.05 V and is followed by another reduction process commencing at -0.3 V. The first peak possibly relates to an adsorption/passivation process followed by the deposition of Zn. However, in the anodic scan, no clear oxidation/dissolution of Zn takes place. Only, a small oxidation peak is observed at 0.1 V which can be related to the oxidation of electrodeposited Zn. However, compared to Figure 5a, no prominent reduction and oxidation peaks are observed. This observation can be related to the difference in Zn coordination observed in Figure 4. For BetOAc, as Zn is coordinated with five acetate ions, the Zn reduction process occurs at a more negative potential compared to ChOAc. Furthermore, the absence of the oxidation process suggests that besides the coordination, the presence of Betaine influences the Zn electrochemistry.

This also is further evidenced by studying the Zn/Zn symmetric cell in the two electrolytes. Figure 5c shows the Zn deposition/stripping in ChOAc-based electrolyte wherein a stable deposition and stripping potential is observed for 70 hours and the SEM image (Figure S3) shows a dendrite-free deposition of Zn. However, it is evident from Figure 5d that Zn

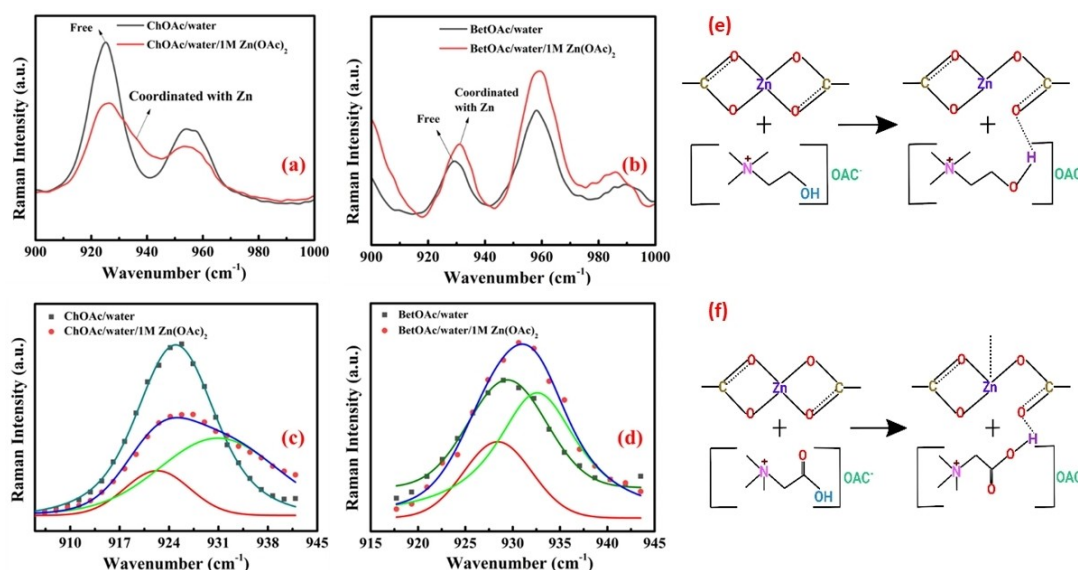


**Figure 4.** (a) Raman spectra comparison of ChOAc/water and ChOAc/water/1 M  $\text{Zn}(\text{OAc})_2$  (b) Raman spectra comparison of BetOAc/water and BetOAc/water/1 M  $\text{Zn}(\text{OAc})_2$  (c) Deconvolution of Raman spectra for ChOAc electrolyte (d) Deconvolution of Raman spectra for BetOAc electrolyte. (e, f) The chemical structure of  $\text{Zn}(\text{OAc})_2$  and its reaction with ChOAc and BetOAc.

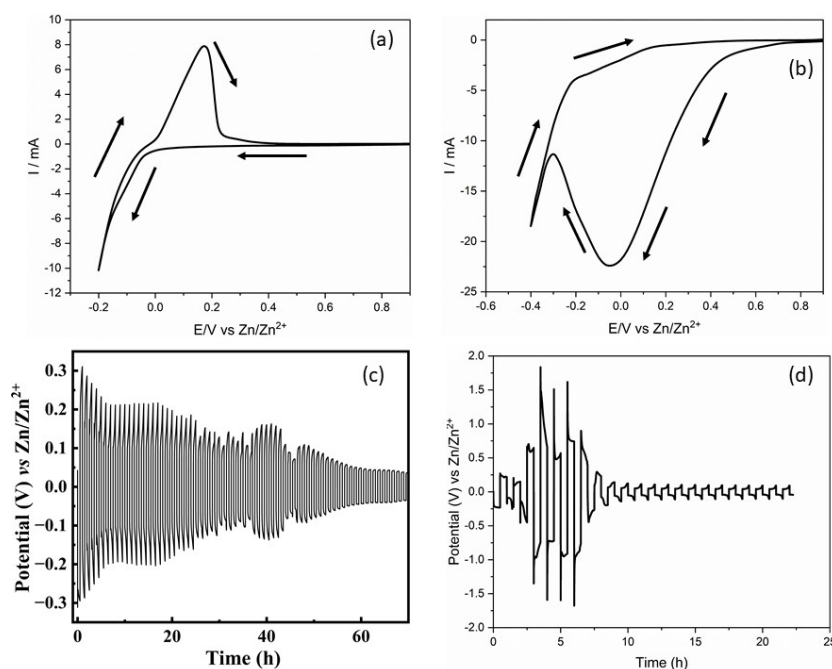


**Figure 5.** CV of Zn electrodeposition on Cu from (a) 80% ChOAc/water/1 M Zn(OAc)<sub>2</sub> (b) 80% BetOAc/water/1 M Zn(OAc)<sub>2</sub> (c) Charge/discharge profile of Zn deposition/stripping in ChOAc based electrolyte at 0.5 mA cm<sup>-2</sup> with a capacity of 0.5 mAh cm<sup>-2</sup> (d) Charge/discharge profile of Zn deposition/stripping in BetOAc based electrolyte at 0.5 mA cm<sup>-2</sup> with a capacity of 0.5 mAh cm<sup>-2</sup>.

deposition/stripping is not steady in BetOAc-based electrolytes which can be attributed to difficulty in nucleation and growth of Zn. Based on the spectroscopic and electrochemical analyses, it is evident that Choline is a more suitable cation for Zn ion capacitors. Therefore, further electrochemical studies were carried out with 80% ChOAc/water/1 M Zn(OAc)<sub>2</sub> electrolyte.

#### Asymmetric AC/Zn SC Devices with 80% ChOAc/Water/1 M Zn(OAc)<sub>2</sub> System

A capacitor-type cathode (AC) and a battery-type anode (Zn) were used to construct an asymmetric battery-SC type hybrid device using 80 percent ChOAc/water/1 M Zn(OAc)<sub>2</sub> electrolyte. The open circuit voltage was found to be 1.2 V. All the CVs (Figure 6a) were performed in the voltage range of 0.3 V–2.0 V at different scan rates of 1–100 mVs<sup>-1</sup>. The CV curves for asymmetric devices show a redox process at 1.2/1.0 V which was not observed in the symmetric SCs. The redox process can be related to some Zn interaction with activated carbon. To evaluate the charging and discharging capacity of the device, the GCD was carried out at a current density of 0.1–1 Ag<sup>-1</sup> in the potential range of 0.3–2 V (Figure 6b). The charge-discharge curves do not show a typical supercapacitor triangular behaviour, but shows the feature of a hybrid capacitor where Zn<sup>2+</sup> ions are reduced on the Zn anode whereas OAc<sup>-</sup> anions are adsorbed/intercalated on the AC cathode during charging and the opposite process takes place during discharge.<sup>[53]</sup>

The GCD profile calculated at different current densities is shown in Figure 6c. The  $C_{\text{spec,cell}}$  of a symmetric SC device at current densities of 0.1, 0.2, 0.3, 0.5, 1, 2 and 3 Ag<sup>-1</sup> are 95, 63,

50, 36, 20 and 15 Fg<sup>-1</sup>, respectively. The error estimation of the specific capacitance was  $\pm 4$  Fg<sup>-1</sup>. At higher current densities the capacity drops significantly which may be due to side reactions taking place at higher current density. The specific energy densities and power densities calculated from the GCD curve show that the Zn/AC hybrid device delivered a specific energy density of 37.2 Whkg<sup>-1</sup> and a power density of 135 Wkg<sup>-1</sup> at 0.1 Ag<sup>-1</sup>. The obtained energy density data were comparable with AC-based aqueous and organic electrolytes-based SCs which showed a value between 10 and 70 Wh kg<sup>-1</sup>.<sup>[54–59]</sup> Finally, the stability of the ZIC in 80% ChOAc/water/1 M Zn(OAc)<sub>2</sub> electrolyte was evaluated at a current density of 0.5 Ag<sup>-1</sup> which shows a capacity close to 40 Fg<sup>-1</sup> with about 82% capacity retention after 3000 cycles (Figure 6e). Thus, these results pave new direction in developing sustainable and biodegradable ZIC.

## Conclusions

In summary, we have studied bio-ionic liquids as electrolytes for Zn-ion capacitors and have evaluated the cation effect of bio-ILs (ChOAc and BetOAc) on symmetric and asymmetric supercapacitors. For symmetric cells, a higher capacitance was observed using BetOAc. The presence of Zn acetate in the electrolyte changed the electrochemical behaviour significantly. IR and Raman studies showed that zinc solvation changes significantly depending on the cation which affects the electrochemical reactions. Based on the Raman, IR and electrochemical analyses, it was evident that choline was a more suitable cation than betaine for Zn ion capacitors. Furthermore, at 0.1 Ag<sup>-1</sup>

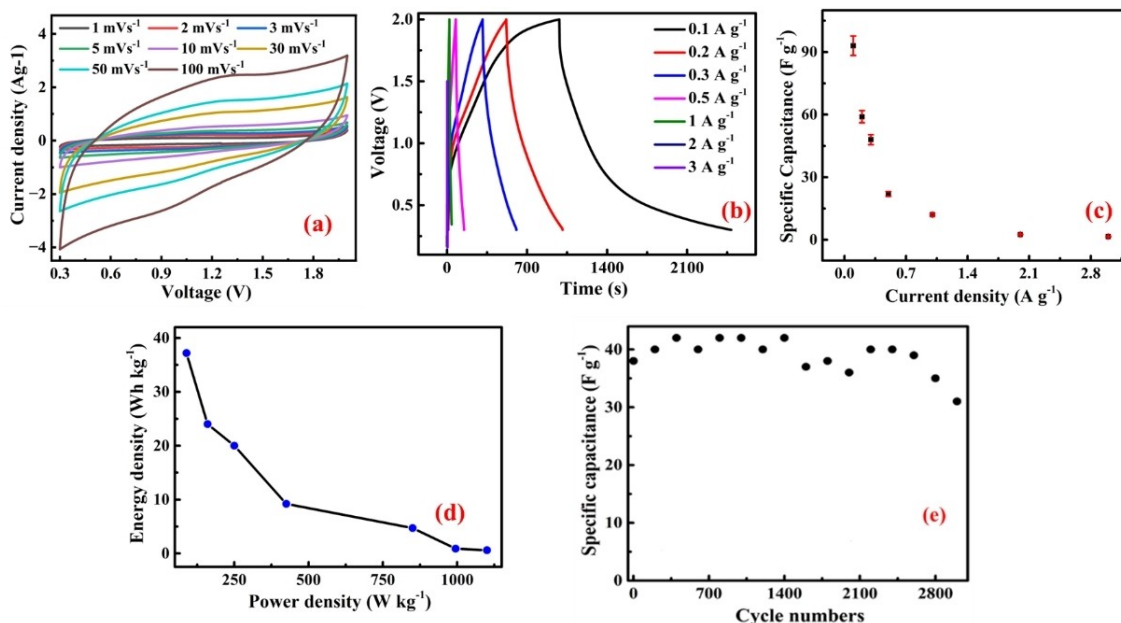


**Figure 6.** (a) CV curve at different scan rates (b) GCD profile at different current densities (c) The specific capacity as a function of different current densities and (d) Ragone plot and (e) Plot of discharge capacity vs. cycle numbers of AC/Zn hybrid capacitor in 80% ChOAc/water/1 M Zn(OAc)<sub>2</sub>.

current density, the Zn/AC hybrid device gave an energy density of 37.2 Whkg<sup>-1</sup> corresponding to a power density of 135 Wkg<sup>-1</sup>. At a current density of 0.5 Ag<sup>-1</sup>, the hybrid SC device shows a long cycle life and retains 82% specific capacitance even after 3000 cycles.

## Acknowledgements

We thank EPSRC, EP/W015129/1 for funding this research.

## Conflict of Interests

The authors declare no conflict of interest.

## Data Availability Statement

The data that support the findings of this study are openly available in Figshare at 10.17633/rd.brunel.24635118, reference number 24635118.

**Keywords:** Bio ionic liquids · Zn solvation · Cation effect · Zinc ion capacitor · Symmetric capacitor

- [1] J. Sun, B. Luo, H. Li, *Adv. Energy Sust. Res.* **2022**, *3*, 2100191–2100217.
- [2] L. Wang, M. Peng, J. Chen, T. Hu, K. Yuan, Y. Chen, *Adv. Mater.* **2022**, *34*, 2203744.
- [3] L. Wang, M. Peng, J. Chen, X. Tang, L. Li, T. Hu, K. Yuan, Y. Chen, *ACS Nano* **2022**, *16* (2), 2877–2888.
- [4] C. Han, H. Li, R. Shi, L. Xu, J. Li, F. Kang, B. Li, *Energy Environ. Mater.* **2018**, *1*, 75–87.

- [5] P. Han, G. Xu, X. Han, J. Zhao, X. Zhou, G. Cui, *Adv. Energy Mater.* **2018**, *8*, 1801243–1801273.
- [6] J. Ding, W. Hu, E. Paek, D. Mitlin, *Chem. Rev.* **2018**, *118*, 6457–6498.
- [7] L. Xia, B. Tang, J. Wei, Z. Zhou, *Batteries & Supercaps* **2021**, *4*, 1108–1121.
- [8] Y. Wu, Y. Suna, Y. Tonga, X. Liua, J. Zhenga, D. Han, H. Li, L. Niu, *Energy Storage Mater.* **2021**, *41*, 108–132.
- [9] X. Liu, Y. Sun, Y. Tong, X. Wang, J. Zheng, Y. Wu, H. Li, L. Niu, Y. Hou, *Nano Energy* **2021**, *86*, 106070–106100.
- [10] H. Zhou, C. Liu, J.-C. Wu, M. Liu, D. Zhang, H. Song, X. Zhang, H. Gao, J. Yang, D. De Chen, *J. Mater. Chem. A* **2019**, *7*, 9708–9715.
- [11] Z. Li, Z. Xiong, H. Pan, N. Shang, Y. Gao, *ACS Appl. Energy Mater.* **2023**, *6*, 10554–10563.
- [12] D. Zhang, L. Li, Y. Gao, Y. Wu, J. Deng, *ChemElectroChem* **2021**, *8*, 1541–1557.
- [13] F. Li, X. Hu, *Batteries & Supercaps* **2021**, *4*, 389–406.
- [14] K. Xiao, L. Yang, M. Peng, X. Jiang, T. Hu, K. Yuan, Y. Chen, *Small* **2024**, *20*, 2306808.
- [15] H. Xu, W. He, Z. Li, J. Chi, J. Jiang, K. Huang, S. Li, G. Sun, H. Dou, X. Dou, *Adv. Funct. Mater.* **2022**, *32*, 2111131–2111140.
- [16] H. Zong, A. Zhang, J. Dong, Y. He, H. Fu, H. Guo, F. Liu, J. Xu, J. Liu, *Chem. Eng. J.* **2023**, *475*, 146088.
- [17] Z. Lu, K. Zhao, H. Guo, L. Duan, H. Sun, K. Chen, J. Liu, *Small* **2023**, *20*, 202309814.
- [18] R. Yuksel, N. Karakehya, *Carbon* **2024**, *221*, 118934–118944.
- [19] P. Naskar, D. Kundu, A. Maiti, P. Chakraborty, B. Biswas, A. Banerjee, *Chem. Electro. Chem. Rev.* **2021**, *8*, 139–1429.
- [20] S. Wu, Y. Chen, T. Jiao, J. Zhou, J. Cheng, B. Liu, S. Yang, K. Zhang, W. Zhang, *Adv. Energy Mater.* **2019**, *9*, 1902915–1902922.
- [21] L. Kang, M. Cui, Z. Zhang, F. Jiang, *Batteries & Supercaps* **2020**, *3*, 966–1005.
- [22] Y. Xu, X. Zheng, J. Sun, W. Wang, M. Wang, Y. Yuan, M. Chuai, N. Chen, H. Hu, W. Chen, *Nano Lett.* **2022**, *22*, 3298–3306.
- [23] H. Yuan, H. Shimotani, A. Tsukazaki, A. Ohtomo, M. Kawasaki, Y. Iwasa, *J. Am. Chem. Soc.* **2010**, *132*, 6672–6678.
- [24] O. Borodin, G. A. Giffin, A. Moretti, J. B. Haskins, J. W. Lawson, A. Wesley, W. A. Henderson, S. Passerini, *J. Phys. Chem. C* **2018**, *122*, 20108–20121.
- [25] D. R. MacFarlane, N. Tachikawa, M. Forsyth, J. M. Pringle, P. C. Howlett, G. D. Elliott, J. H. Davis, M. Watanabe, P. Simon, C. A. Angell, *Energy Environ. Sci.* **2014**, *7*, 232250.
- [26] X. Li, C. Cai, L. Zhou, L. Mai, H. J. Fan, *Adv. Mater.* **2022**, 2202380.
- [27] Z. Liu, S. Z. El. Abedina, F. Endres, *Phys. Chem. Chem. Phys.* **2015**, *17*, 15945–15952.
- [28] F. Ilyas, M. Ishaq, M. Jabeen, M. Saeed, A. Ihsan, M. Ahmed, *J. Mol. Liq.* **2021**, *343*, 117606–117626.

- [29] K. A. Fletcher, S. Pandey, *J. Phys. Chem. B* **2003**, *107*, 13532–13539.
- [30] K. R. Seddon, A. Stark, M. Torres, *J. Pure Appl. Chem.* **2000**, *72*, 2275–2287.
- [31] J. Chen, W. Zhou, Y. Quan, B. Liu, M. Yang, M. Chen, X. Han, X. Xu, P. Zhang, S. Shi, *Energy Storage Mater.* **2022**, *53*, 629–637.
- [32] L. Miao, Z. Song, D. Zhu, L. Li, L. Gan, M. Liu, *Energ. Fuel* **2021**, *35*, 8443–8455.
- [33] B. Kanjilal, Y. Zhu, V. Krishnados, J. M. Unagolla, P. Saemian, A. Caci, D. Cheraghali, I. Dehzangi, A. Khademhosseini, I. Noshadi, *Adv. Intell. Syst.* **2023**, *5*, 2200306.
- [34] M. Sharma, D. Mondal, R. Alphons Sequeira, R. K. Talsaniya, D. A. Marua, K. Moradiyaa, K. Prasad, *J. Indian Chem. Soc.* **2021**, *98*, 100205.
- [35] I. Noshadi, B. W. Walker, R. Portillo-Lara, E. Shirzaei Sani, N. Gomes, M. Reza Aziziyan, N. Annabi, *Sci. Rep.* **2017**, *7*, 4345.
- [36] M. Mokhtarpour, N. Basteholia, H. Shekaari, M. Taghi, Z. Moattar, *J. Mol. Liq.* **2020**, *306*, 112504–112514.
- [37] P. D. Diabate, S. Boudesocque, A. Mohamadou, L. Dupont, *Sep. Purif. Technol.* **2020**, *244*, 11678–11688.
- [38] W. Kao-ian, R. Pornprasertsuk, P. Thamyongkit, T. Maiyalagan, S. Kheawhom, *J. Electrochem. Soc.* **2019**, *166* (6), 1063–A1069.
- [39] A. Lahiri, L. Yang, O. Hoff, F. Endres, *Mater Adv* **2021**, *2*, 2676.
- [40] Y. Jing, F. Ning, Z. Jing, L. Rui, L. Feng, D. Yuchuan, Y. Zhenglong, *ACS Omega* **2019**, *4*, 15904–15911.
- [41] S. Brahma, K. Ramanujam, R. L. Gardas, *Ind. Eng. Chem. Res.* **2022**, *61*, 12073–12082.
- [42] Y. Zheng, Y. Zheng, Q. Wang, Z. Wang, *J. Chem. Eng. Data* **2021**, *66*, 480–493.
- [43] M. Liu, H. Xiao, R. Pan, J. Ren, L. Zhang, L. Zhang, *Langmuir* **2024**, *40*, 6898–6908.
- [44] A. Ray, B. Saruhan, *Materials* **2021**, *14*, 2942.
- [45] J. Feng, X. Yan, Y. Wang, Y. Xu, Y. Sun, Y. Tang, *Energy Environ. Sci.* **2021**, *14*, 2859.
- [46] M. K. Johnson, D. B. Powell, R. D. Cannon, *Spectrochim. Acta* **1981**, *37A*, 899–904.
- [47] A. Pawlukojć, L. Hetmańczyk, *Chem. Phys.* **2014**, *445*, 31–37.
- [48] M. S. Ghazvini, G. Pulletikurthi, A. Lahiri, F. Endres, *ChemElectroChem* **2016**, *3*, 598–604.
- [49] P. Duan, Q. Xu, X. Zhang, J. Chen, W. Zheng, L. Li, J. Yang, F. Fu, H. Diao, X. Liu, *Cellulose* **2020**, *27*, 6603–6615.
- [50] M. I. Cabaço, M. Besnard, Y. Danten, J. A. P. Coutinho, *J. Phys. Chem. B* **2011**, *115*, 3538–3550.
- [51] T. J. Simons, A. A. J. Torriero, P. C. Howlett, D. R. MacFarlane, M. Forsyth, *Electrochem. Commun.* **2012**, *18*, 119–122.
- [52] Z. Liu, T. Cui, T. Lu, M. S. Ghazvini, F. Endres, *Phys. Chem. Chem. Phys.* **2016**, *120*, 20224–20231.
- [53] M. Peng, X. Tang, K. Xiao, T. Hu, K. Yuan, Y. Chen, *Angew. Chem. Int. Ed.* **2023**, *62* (27), e202302701.
- [54] S. Brahma, K. Ramanujam, *Ionics* **2022**, *28*, 1427–1440.
- [55] H. Wanga, M. Wanga, Y. Tanga, *Energy Storage Mater.* **2018**, *13*, 1–7.
- [56] T. Xiong, Y. Shen, W. S. V. Lee, J. Xue, *Nano Mater. Sci.* **2020**, *2*, 159.
- [57] D. L. Han, S. C. Wu, S. W. Zhang, Y. Q. Deng, C. J. Cui, L. A. Zhang, Y. Long, H. Li, Y. Tao, Z. Weng, Q. H. Yang, F. Y. Kang, *Small* **2020**, *16* (29), 2001736.
- [58] L. Dong, X. Ma, Y. Li, L. Zhao, W. Liu, J. Cheng, C. Xu, B. Li, Q.-H. Yang, F. Kang, *Energy Storage Mater.* **2018**, *13*, 96–102.
- [59] Z. Zou, X. Luo, L. Wang, Y. Zhang, Z. Xu, C. Jiang, *J. Energy Storage* **2021**, *44*, 103385.

Manuscript received: August 27, 2024  
Revised manuscript received: October 2, 2024  
Version of record online: November 13, 2024